doi:10.3772/j.issn.1006-6748.2021.02.009

Optimal design and experiment research of an orthogonal-parallel six-axis force/torque sensor①

Wang Zhijun(王志军)[*,**], Liu Lu[*,**], Cui Bingyan[*,**], He Jing②[***], Li Zhanxian[*,**]
([*] College of Mechanical Engineering, North China University of Science and Technology, Tangshan 063210, P. R. China)
([**] Hebei Province Research Institute of Industrial Robot Industry Technology, Tangshan 063210, P. R. China)
([***] Tangshan Industrial Vocational Technical College, Tangshan 063020, P. R. China)

Abstract

A novel orthogonal-parallel six-axis force/torque sensor is studied based on a modified Stewart platform architecture, and the optimal design and experiment research of the sensor are discussed. Firstly, the model of orthogonal parallel six-axis force/torque sensor based on improved Stewart platform architecture and its static mathematical model are proposed. Secondly, according to the actual working condition of the sensor, the sensor is optimized and the optimal solution is obtained. Then, the experimental prototype and calibration system is developed. Finally, the superiority of the sensor structure and the effectiveness of the optimization method are verified by calibration experiments. The results of the proposed method are useful for the further research and application of the orthogonal-parallel six-axis force/torque sensor.

Key words: six-axis force sensor, optimal design, online static calibration, working condition

0 Introduction

With the progress of science and technology, six-axis force/torque sensors have urgent needs and broad application prospects in high-tech fields such as industrial engineering. Six-axis force/torque sensors in the fields of medical treatment and precision assembly are widely used as force sensing information acquisition and transmission devices for intelligent operating systems[1-2]. The research on the theory and calibration test of the six-axis force/torque sensor mechanism plays an important role in the engineering needs of various industries.

In 1983, Stewart platform was applied to the design of six-axis force and torque sensor[3]. Since then, Stewart parallel mechanism has been successfully applied to the design of six-axis force/torque sensor because of its high stiffness, stable structure, strong bearing capacity, no error accumulation, easy to solve inverse kinematics and so on, which has attracted the attention of scholars of many different countries[4]. Six-axis force/torque sensors are required to measure dynamic changes in force accurately and quickly. Therefore, research on the dynamic performance of six-axis force/torque sensors has become very important. Ref. [5] introduced and compared a variety of dynamic calibration methods for force and torque sensors, and proposed levitation mass method (LMM) for dynamic calibration of force sensors. Refs[6,7] proposed a novel self-decoupled piezoelectric six-axis force/torque sensors based on the parallel load sharing principle in order to solve the heavy force measurement technical problem of the piezoelectric six-dimensional force sensor. Ref. [8] applied the force sensor to the dynamic analysis of ski steering, which can be used to evaluate the turning skills. Ref. [9] presented a newly designed six-axis force/moment sensor, whose thickness is reduced to 12 mm. Ref. [10] presented research on static linear and nonlinear decoupling algorithms of piezoelectric six axis force/torque sensor. Ref. [11] developed a novel micro force sensor based on depletion type vertically movable gate array field effect transistor (VMGAFET) with cross-axis decoupling structure and eight gate arrays, which was able to detect ultra-low force and exhibited high measuring sensitivity. Ref. [4] introduced a six-axis force sensor with parallel 8/4-4 structure and analyzed its measurement principle.

The Stewart platform parallel structure cannot realize the 6-dimensional force measurement of stress

① Supported by the National Natural Science Foundation of China (No. 51505124), Foster Fund Projects of North China University of Science and Technology (No. JP201505), the Science and Technology Research Project of Hebei Province (No. ZD2020151).
② To whom correspondence should be addressed. E-mail: hejing409@126.com
Received on Apr, 11, 2020

coupling between the sensitive elements[12-13]. The pre-stressed multi-limb six-axis force sensor both keeps the advantages of Stewart platform parallel structure and greatly overcomes the main disadvantages previously mentioned. An orthogonal-parallel six-axis force/torque sensor is proposed, and the optimal design and experiment research are discussed. The aim is to find an evaluation criterion to develop six-axis force/torque sensor that can be applied to a certain task. In addition, it is practically significant to research on the experiment of the proposed sensor for authenticating the optimization method.

1 Orthogonal-parallel six-axis force/torque sensor

1.1 Structure of the orthogonal-parallel six-axis force/torque sensor

The novel orthogonal-parallel six-axis force/torque sensor based on a modified Stewart platform architecture is shown in Fig. 1. It is mainly composed of a force measuring platform, a base platform, six force measuring limbs and six supporting beams. A strain gauge is attached to the middle of each force measuring limb to detect the axial force acting on the limb. The vertical and horizontal force measuring limbs are circularly symmetrical with respect to the central axis of the base platform. The two ends of three vertical force measuring limbs are connected with base platform and force measuring platform through elastic spherical joints. The other three horizontal force measuring limbs are connected with the supporting beams on the base platform and the force measuring platform through elastic spherical joints, and the axes of the limbs do not intersect at the same point.

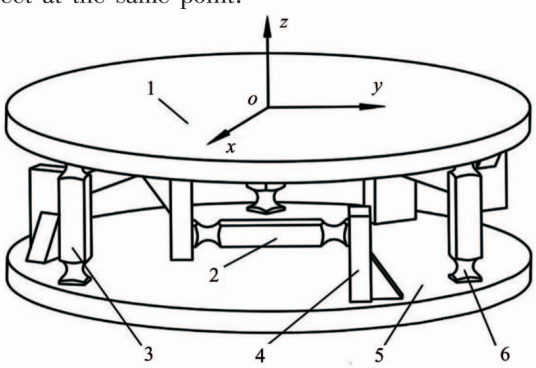

1. measuring platform; 2. horizontal measuring limb; 3. vertical measuring limb; 4. supporting beam; 5. base platform; 6. elastic spherical joint

Fig. 1 The orthogonal-parallel six-axis force/torque sensor

The two ends of the force measuring limb of the six-axis force sensor are both elastic spherical joints. Ideally, the force measuring limb can be regarded as two-force rods, so it only bears axial force. Because the limbs of force measurement are arranged horizontally and vertically in space, they can be measured by three force limbs arranged horizontally when the applied force is X-direction force, Y-direction force and Z-direction torque. Similarly, when the applied force is Z-direction force, X-direction torque and Y-direction torque, they can be measured by three vertical measuring limbs respectively. So, the orthogonal-parallel six-axis force/torque sensor not only realizes the accurate measurement of six-axis external force in principle, but also is decoupled to a certain extent.

1.2 Static mathematical model of the force sensor

As a foundation for the structural parameters optimization, the static mathematical model of the orthogonal-parallel six-axis force/torque sensor should be built firstly. As shown in Fig. 2, the measuring coordinate frame $\{M\}$ is attached to the geometric center of the force measuring platform. And the symbols are defined as follows. $\boldsymbol{b}_i$ and $\boldsymbol{B}_i$ $(i=1, 2, 3)$ denote the position vectors of the ith spherical joint of the vertical force measuring limbs about the coordinate frame with circularly-symmetric distribution. $\boldsymbol{b}_j$ and $\boldsymbol{B}_j$ $(j=4, 5, 6)$ denote the position vectors of the jth spherical joint of the horizontal force measuring limbs about the coordinate frame with circularly-symmetric distribution. The structural parameters of the sensor are defined as follows. a_1 denotes the radius of the circle with which the center of spherical joints ($\boldsymbol{b}_i$ and $\boldsymbol{B}_i$) located at the pre-stressing platform and base platform, a_2 denotes the radius of the inscribed circle by Line $\boldsymbol{B}_4\boldsymbol{b}_4$, $\boldsymbol{B}_5\boldsymbol{b}_5$ and $\boldsymbol{B}_6\boldsymbol{b}_6$. a_3 is the vertical distance between the plane determined by the horizontal force measuring limbs and

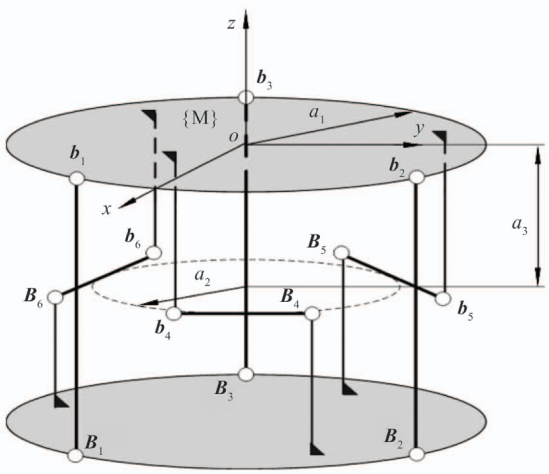

Fig. 2 Schematic drawing of the orthogonal-parallel six-axis force sensor

the measuring platform. l denotes the length the measuring limb. The origin of the measuring coordinate frame $\{M\}$ is established in the plane geometric center of the force measuring platform. The X-axis is in the plane of the force measuring platform and perpendicular to the line $\boldsymbol{B}_4\boldsymbol{b}_4$. The Z-axis is perpendicular to the force measuring platform and sticking straight up.

For the equilibrium of the force measuring platform, the following equation can be obtained as

$$\sum_{i=1}^{n} f_i \$_i = \boldsymbol{F} + \in \boldsymbol{M} \tag{1}$$

where $\boldsymbol{F}$ and $\boldsymbol{M}$ represent the applying force vector and torque vector acted on the coordinate center of the force measuring platform, respectively; $\in$ is the dual sign; $f_i (i = 1, 2, \cdots, 6)$ represents the force produced on the ith measuring limb; $\$_i$ represents the unit line vector along the ith measuring limb, and $\$_i = \boldsymbol{S}_i + \in \boldsymbol{S}_{0i}$, $\boldsymbol{S}_i \cdot \boldsymbol{S}_i = 1$, $\boldsymbol{S}_i \cdot \boldsymbol{S}_{0i} = 0$, $\boldsymbol{S}_{0i} = \boldsymbol{r} \times \boldsymbol{S}_i$; $\boldsymbol{r}_i$ is the position vector of a point on the ith measuring limb.

Eq. (1) can be rewritten as

$$\boldsymbol{F}_w = \boldsymbol{G} \cdot \boldsymbol{f} \tag{2}$$

where $\boldsymbol{F}_w = [F_x \quad F_y \quad F_z \quad M_x \quad M_y \quad M_z]^T$ is the vector of six-dimension external force applied on the measuring platform, $\boldsymbol{f} = [f_1 \quad f_2 \quad \cdots \quad f_6]^T$ is the vector composed of the forces of the measuring limbs, $\boldsymbol{G}$ is the force Jacobin matrix which is given by

$$\boldsymbol{G} = \begin{bmatrix} \dfrac{\boldsymbol{b}_1 - \boldsymbol{B}_1}{|\boldsymbol{b}_1 - \boldsymbol{B}_1|} & \dfrac{\boldsymbol{b}_1 - \boldsymbol{B}_1}{|\boldsymbol{b}_1 - \boldsymbol{B}_1|} & \cdots & \dfrac{\boldsymbol{b}_6 - \boldsymbol{B}_6}{|\boldsymbol{b}_6 - \boldsymbol{B}_6|} \\ \dfrac{\boldsymbol{b}_1 \times \boldsymbol{B}_1}{|\boldsymbol{b}_1 - \boldsymbol{B}_1|} & \dfrac{\boldsymbol{b}_1 \times \boldsymbol{B}_1}{|\boldsymbol{b}_1 - \boldsymbol{B}_1|} & \cdots & \dfrac{\boldsymbol{b}_6 \times \boldsymbol{B}_6}{|\boldsymbol{b}_6 - \boldsymbol{B}_6|} \end{bmatrix} \tag{3}$$

Substituting the structural parameters of the sensor into Eq. (3), Eq. (4) can be obtained:

$$\boldsymbol{G} = \begin{bmatrix} 0 & 0 & 0 & 0 & \dfrac{\sqrt{3}}{2} & -\dfrac{\sqrt{3}}{2} \\ 0 & 0 & 0 & -1 & \dfrac{1}{2} & \dfrac{1}{2} \\ 1 & 1 & 1 & 0 & 0 & 0 \\ -\dfrac{\sqrt{3}}{2}a_1 & \dfrac{\sqrt{3}}{2}a_1 & 0 & -a_3 & \dfrac{a_3}{2} & \dfrac{a_3}{2} \\ -\dfrac{a_1}{2} & -\dfrac{a_1}{2} & a_1 & 0 & -\dfrac{\sqrt{3}}{2}a_3 & \dfrac{\sqrt{3}}{2}a_3 \\ 0 & 0 & 0 & -a_2 & -a_2 & -a_2 \end{bmatrix} \tag{4}$$

Eq. (4) shows that the dimension column vectors in $\boldsymbol{G}$ are not correlated, that is, the sensor is not in a singular configuration at this time, and the six-axis force/torque can be determined solely by the axial force of measuring limbs. Eq. (4) shows that when the external force applied on the sensor is F_x, it can be measured by the 5th and 6th measuring limbs. When the external force is F_y or M_z, it can be measured by the 4th, 5th and 6th measuring limbs. When the external force is F_z or M_y, it can be measured by the 1st, 2nd and 3rd measuring limbs. When the external force is M_x, it can be measured by the 1st and 2nd measuring limbs. So, because of the special layout of force measuring limbs, the decoupling performance of six-axis force/torque sensor has been greatly improved.

The mapping relation between the six-dimension external force and the reacting forces of the six measuring limbs can be given as

$$\boldsymbol{f} = \boldsymbol{G}^{-} \boldsymbol{F}_w \tag{5}$$

where, $\boldsymbol{G}^{-}$ is the inverse matrix for the force Jacobin matrix $\boldsymbol{G}$.

So far, the mapping relationship between the six-dimension external force and the reacting forces of the six measuring limbs is obtained, and static equilibrium equation of the orthogonal-parallel six-axis force/torque sensor is solved.

2 Optimal design of the orthogonal-parallel six-axis force/torque sensor

2.1 Working condition function of the force sensor

Before optimizing the structural parameters of the sensor, the measurement requirement, i. e. the working condition, should be defined so as to design and optimize the structure pertinently.

Six-axis force/torque sensor is usually installed on the wrist of a robot. The six-dimension external force $\boldsymbol{F}_w$ applied on the sensor varies with time. Let the working cycle time of the robot to complete a task be T, and $\boldsymbol{F}_w$ be a function of time, which can be expressed as

$$\boldsymbol{F}_w(t) = [\boldsymbol{F}_x(t) \quad \boldsymbol{F}_y(t) \quad \boldsymbol{F}_z(t) \quad \boldsymbol{M}_x(t) \quad \boldsymbol{M}_y(t) \quad \boldsymbol{M}_z(t)]^T \tag{6}$$

where, $\boldsymbol{F}_w(t)$ is the working condition function, which can fully show the force/torque on the wrist when the robot works normally.

Combining with engineering practice, it is easy to know that the six-dimension external force on the wrist of a robot in normal working space should be a vector varying with time. Therefore, all items in F_w should be defined as bounded functions within the working period T.

Substituting Eq. (6) into Eq. (5), the function expression of the axial reaction force produced by the force measuring limb under the action of external force is

$$\boldsymbol{f}_{\mathrm{w}}(t) = \boldsymbol{G}^{-}\boldsymbol{F}_{\mathrm{w}}(t) = [f_{1\mathrm{w}}(t) \quad f_{2\mathrm{w}}(t) \quad \cdots \quad f_{6\mathrm{w}}(t)]^{\mathrm{T}} \tag{7}$$

where $f_{iw}(t)(i = 1, 2, \cdots, 6)$ is the axial reaction force function of the ith measuring limb. $f_{iw}(t)$ is also a bounded function in the working period T.

Within the definition domain of $I = [0, T]$, for the reaction force function of the ith force measuring leg $f_{iw}(t)$, the following inequality holds when $t_{i0} \in I$ and $t_{i1} \in I$.

$$f_{iw}(t_{i0}) \geqslant f_{iw}(t) \geqslant f_{iw}(t_{i1}) \quad i = 1, 2, \cdots, 6 \tag{8}$$

It is shown that there are maximum $f_{iw\max} = f_{iw}(t_{i0})$ and minimum $f_{iw\min} = f_{iw}(t_{i1})$ surely of the reaction force function $f_{iw}(t)$ within its definition field $I = [0, T]$. For the six measuring limbs, the maximum absolute value f_m can be compared with the value of $|f_{iw\max}|$ and $|f_{iw\min}|$. Therefore, if the range of the measuring limb M satisfies $M \supseteq [f_m, -f_m]$, the sensor can be used to measure the task six-dimension force represented by the working condition function.

2.2 Optimal design based on the working condition function

When the sensor satisfies the working condition function model, the structure optimization is carried out with the aim of reducing the range of force measuring limb. The optimized six-axis force/torque sensor structure can not only minimize the range of force measuring limb, but also have better mechanical and measuring performance under this working condition.

Assuming that the array consisting of each structural parameter of the sensor is $\boldsymbol{\delta} = [\delta_1 \quad \cdots \quad \delta_k]$. The range of structural parameters of the sensor can be obtained according to the size of the installation space. $\boldsymbol{N} = [N_1 \quad \cdots \quad N_k]$ is an array composed by the range of structural parameters. $\boldsymbol{\lambda} = [\lambda_1 \quad \cdots \quad \lambda_k]$ is the step-size array corresponding to the items in the array $\boldsymbol{N}$. Then, the structural parameter $\boldsymbol{\delta}$ in interval $\boldsymbol{N}$ can be calculated step by step according to step $\boldsymbol{\lambda}$, and the mapping matrix $\boldsymbol{G}^{-}$ can be obtained by combining the parameters through different arrangements.

According to the working condition function model, substituting $\boldsymbol{G}^{-}$ and $\boldsymbol{F}_{\mathrm{w}}(t)$ into Eq. (7), the maximum absolute value $\boldsymbol{f}_m$ can be found within its interval. The search aim is to find the minimum value f_0 in $\boldsymbol{f}_m$. Moreover, the array of structural parameters corresponding to f_0 can be obtained, which is expressed as $\boldsymbol{\delta}_0$.

Finally, the minimum range of the measuring limbs of the sensor satisfying the working condition function is obtained by search operation. At the same time, $\boldsymbol{\delta}_0$ determines the sensor structure with the minimum limb range of force measurement as the optimization objective under the working condition function.

2.3 Structural optimization design results

The structural parameters of the orthogonal parallel six-axis force/torque sensor used for the six-dimensional surface grinding operation of industrial robots are optimized based on the working condition function model.

It is known that the working period T of the surface grinding operation of six-degree of freedom (DOF) industrial robot is 23 s. The space contact external force and moment function, i.e., working condition function are given as shown in Fig. 3 and Fig. 4. The objective of optimizing the structural parameters of the six-axis force/torque sensor is to adapt to the requirements of changing external force and moment detection in the working process.

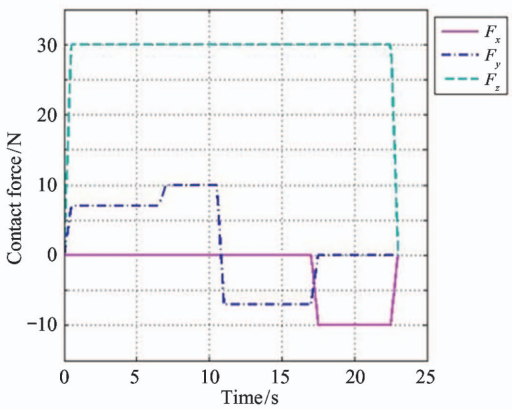

Fig. 3 Function curve of contact force of surface grinding operation

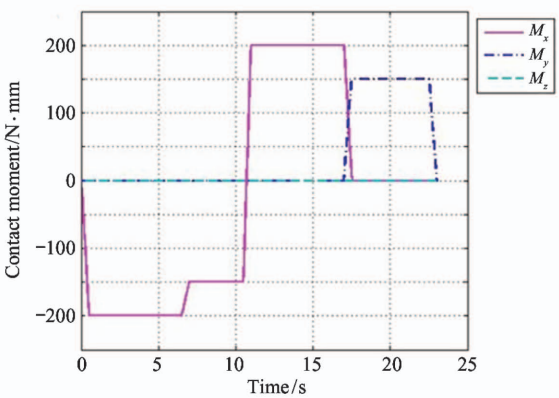

Fig. 4 Function curve of contact moment of surface grinding operation

Based on the theoretical analysis discussed above, a number of structural parameters should be considered in the optimal design of the fully pre-stressed six-axis force/torque sensor, which include radii of the circle

(a_1, a_2) and the vertical distance (a_3).

To simplify the calculation, a_3 is set to be 15 mm. The structural parameter array can be expressed as $\boldsymbol{\delta} = [a_1 \quad a_2]$. The array of the structural parameters range can be expressed as $\boldsymbol{N} = [N_1 \quad N_2]$, where 20 mm $\leqslant N_1 \leqslant$ 50 mm, 20 mm $\leqslant N_2 \leqslant$ 50 mm. The step-size array is $\boldsymbol{\lambda} = [1 \quad 1]$.

Then, the structure parameter $\boldsymbol{\delta}$ is assigned to the mapping matrix $\boldsymbol{G}^-$ according to the step size $\boldsymbol{\lambda}$ in the interval. The axial reaction force measured by the limbs can be solved by substituting the working condition function and the mapping matrix into Eq. (7).

According to Eq. (7), the maximum axial reaction force of measuring limbs under each group of structural parameters is obtained. Finally, a 3-D surface figure is generated to express the relationship between the maximum forces of the measuring limbs and the structural parameters a_1 and a_2 of the sensor, which is shown in Fig. 5.

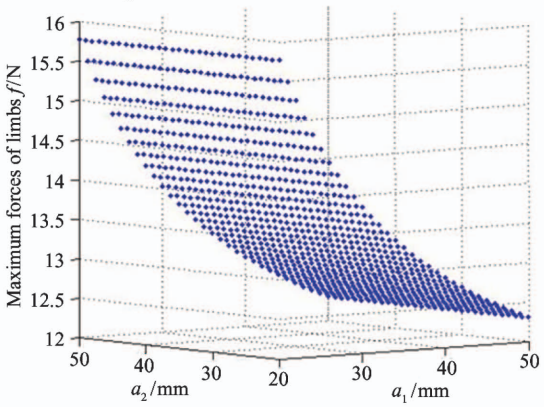

Fig. 5 Mapping of the maximum forces on the measuring limbs respect to the structural parameters a_1 and a_2

In order to minimize the measurement range of the force limb, a search is carried out in the calculation results. Based on the optimization mappings, the final structural parameters and the minimum range of force limb of the sensor prototype are obtained as shown in Table 1, which is suitable for the given working condition.

Table 1 The optimized values of the structural parameters and the force limb range of the sensor

Structural parameters/mm			Force limb range/N
a_1	a_2	a_3	
50	20	15	12.4

3 Calibration experiment

3.1 Sensor prototype and calibration system

In order to investigate the validity of the proposed optimization method, a prototype of the orthogonal-parallel six-axis force/torque sensor is developed. Fig. 6 shows the prototype of the measuring limb, which is also an integrated single-axis strain force sensor with the measurement range of 20 N. Fig. 7 shows the prototype of the proposed orthogonal-parallel six-axis force/torque sensor with structural parameters as the structural optimization result.

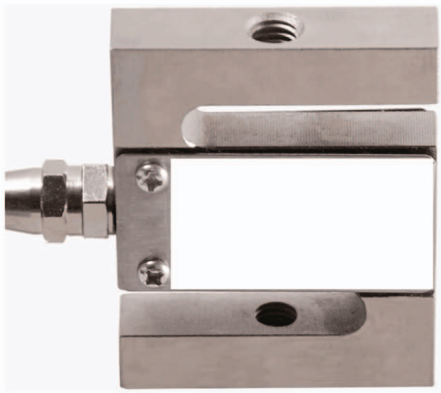

Fig. 6 Photograph of the measuring limb

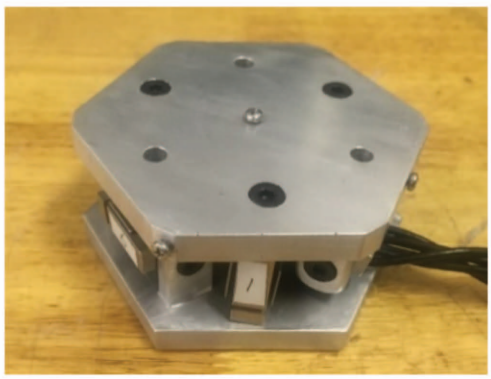

Fig. 7 Photograph of the orthogonal-parallel six-axis force/torque sensor

The online static calibration system of the prototype consists of hardware system and software system. The hardware system includes data acquisition card, upper computer, sensor prototype, voltage signal amplifier, 24 V DC voltage stabilized power supply, etc. Fig. 8 shows the measurement system for experimental calibration. The measurement system uses the PCI8923 data acquisition card of Beijing ART company for data acquisition whose main use is AD analog input function with the measurement precision of 13 bits. Online-static calibration software of orthogonal-parallel six-axis force/torque sensor is LabVIEW, whose interface is shown as Fig. 9.

3.2 Decoupling algorithm and error evaluation

When the load is applied on a six-axis force/torque sensor in one component, other components will

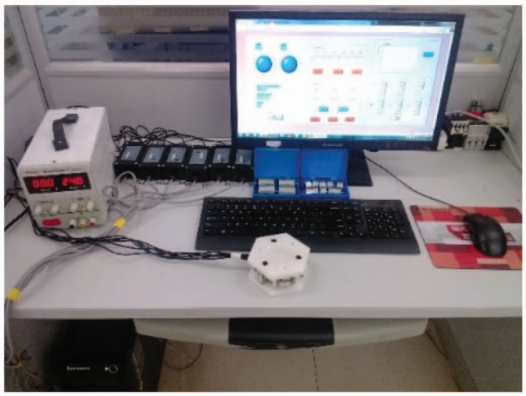

Fig. 8 The measurement system for experimental calibration

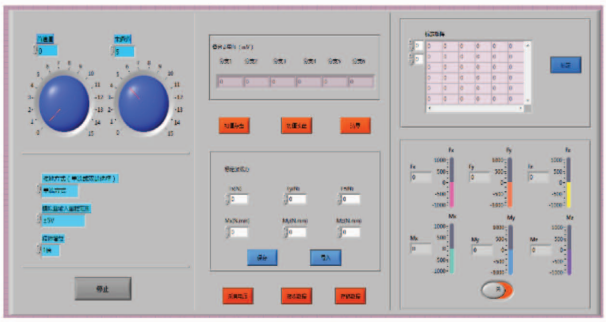

Fig. 9 The interface of calibration software

output force unavoidably, which is named as interference error. In order to reduce the interference error, an effective way is to use calibration matrix to eliminate inter coupling[14]. It can decrease requirement of manufacturing process, and obtain accurate measurement results.

The mapping equation between the applied calibration force/torque and the branch output voltage can be expressed as

$$\boldsymbol{F}_s = \boldsymbol{G}_C \boldsymbol{U} \tag{9}$$

where $\boldsymbol{F}_s$ is the force of Space six-dimensional calibration, $\boldsymbol{U}$ is the output voltage of the measuring limb, $\boldsymbol{G}_c$ is the mapping matrix between the calibration force and the output voltage of the measurement branch. In the measuring range of each direction of the six-dimensional force sensor, it is divided into m loading points, which are successively loaded in a certain order, and then unloaded in reverse order. The standard loading force matrix on six axes can be expressed as

$$\boldsymbol{F}_s = [\boldsymbol{F}_{sx} \quad \boldsymbol{F}_{sy} \quad \boldsymbol{F}_{sz} \quad \boldsymbol{M}_{sx} \quad \boldsymbol{M}_{sy} \quad \boldsymbol{M}_{sz}] \tag{10}$$

where $\boldsymbol{F}_{sx}$, $\boldsymbol{F}_{sy}$, $\boldsymbol{F}_{sz}$, $\boldsymbol{M}_{sx}$, $\boldsymbol{M}_{sy}$, $\boldsymbol{M}_{sz}$ are the calibration force/torque matrix in the corresponding direction, whose order is $6 \times 2m$. The calibration force matrix $\boldsymbol{F}_s$ is a $6 \times 12m$ order matrix.

After applying the calibration force of $12m$ times to the six-dimensional force sensor, the matrix of the corresponding measured branch output voltage is $\boldsymbol{U}$, and when the number of measurement branches is n, the output voltage matrix $\boldsymbol{U}$ is $n \times 12m$ order. The pseudo-inverse matrix of the output voltage matrix $\boldsymbol{U}$ of the measurement branch is multiplied to the left and right sides of Eq. (9), which can be obtained as

$$\boldsymbol{G}_c = \boldsymbol{F}_s \boldsymbol{U}^+ \tag{11}$$

where $\boldsymbol{U}^+$ is the pseudo inverse matrix of $\boldsymbol{U}$, $\boldsymbol{U}^+ = \boldsymbol{U}^{\mathrm{T}} (\boldsymbol{U}\boldsymbol{U}^{\mathrm{T}})^{-1}$, $\boldsymbol{G}_c$ is the calibration matrix. Then Eq. (17) is taken into Eq. (9) to get the measured value of the calibration force $\boldsymbol{F}_c$, which can be expressed as

$$\boldsymbol{F}_c = \boldsymbol{F}_s \boldsymbol{U}^+ \boldsymbol{U} \tag{12}$$

where $\boldsymbol{F}_c = [\boldsymbol{F}_{cx}, \boldsymbol{F}_{cy}, \boldsymbol{F}_{cz}, \boldsymbol{M}_{cx}, \boldsymbol{M}_{cy}, \boldsymbol{M}_{cz}]$, each item in $\boldsymbol{F}_c$ is a matrix of dimension $6 \times 2m$.

Subtraction of Eq. (9) from Eq. (12) and taking the absolute value, the difference of the standard loading force matrix and the calculated force matrix is obtained, which can be expressed as

$$\begin{aligned} \Delta \boldsymbol{L} &= |\boldsymbol{F}_s - \boldsymbol{F}_c| \\ &= [\Delta \boldsymbol{L}_{Fx} \quad \Delta \boldsymbol{L}_{Fy} \quad \Delta \boldsymbol{L}_{Fz} \quad \Delta \boldsymbol{L}_{Mx} \quad \Delta \boldsymbol{L}_{My} \quad \Delta \boldsymbol{L}_{Mz}] \end{aligned} \tag{13}$$

The deviation can be calculated according to Eq. (13), which is the comprehensive nonlinear deviation in each measurement direction when the sensor is working normally.

The linearity of the sensor in the actual measurement is defined as the ratio of the deviation average of each item of Eq. (13) to the full-scale calibration force or the calibration torque in the corresponding measurement direction. The force linearity formula in the x-direction is calculated as

$$\begin{aligned} \boldsymbol{E}_{LFx} = \Big[& \frac{ave(\Delta \boldsymbol{L}_{Fx1})}{F_{xm}} \quad \frac{ave(\Delta \boldsymbol{L}_{Fx2})}{F_{ym}} \quad \frac{ave(\Delta \boldsymbol{L}_{Fx3})}{F_{zm}} \\ & \frac{ave(\Delta \boldsymbol{L}_{Fx4})}{M_{xm}} \quad \frac{ave(\Delta \boldsymbol{L}_{Fx5})}{M_{ym}} \quad \frac{ave(\Delta \boldsymbol{L}_{Fx6})}{M_{zm}} \Big]^{\mathrm{T}} \end{aligned} \tag{14}$$

where $\Delta \boldsymbol{L}_{Fxi} (i = 1, 2, \cdots, 6)$ is the ith row element in matrix $\Delta \boldsymbol{L}_{Fx}$; $ave(\cdot)$ is the average of all elements in vector $(\cdot)$.

The first term of the vector $\boldsymbol{E}_{LFx}$ in Eq. (14) reflects the linearity of the x-direction when the x-direction calibration force is loaded, and the other 5 terms indicate the coupling linearity of the remaining 5 dimensions with the x-direction when the x-direction calibration force is applied. Similarly, when another 5 dimensional calibration force/torque is applied, the linearity of the calibration main direction and the linearity vector of other dimensional couplings can be calculated. The linearity vector in the actual measurement of the sensor can be obtained by sequentially combining the linearity vectors of different dimensions into a matrix, which can be expressed as

$$\boldsymbol{E}_L = [\boldsymbol{E}_{LFx} \quad \boldsymbol{E}_{LFy} \quad \boldsymbol{E}_{LFz} \quad \boldsymbol{E}_{LMx} \quad \boldsymbol{E}_{LMy} \quad \boldsymbol{E}_{LMz}] \tag{15}$$

where $\boldsymbol{E}_L$ is a 6th-order matrix, and the items on the diagonal are type I errors, which reflect the linearity in the main direction of each measurement; and the items on the non-diagonal are type II errors, which reflect the coupling linearity between different measurement directions. The error generated in the actual measurement of the calibration force/torque loaded in each direction in the calibration experiment can be objectively and comprehensively reflected in $\boldsymbol{E}_L$.

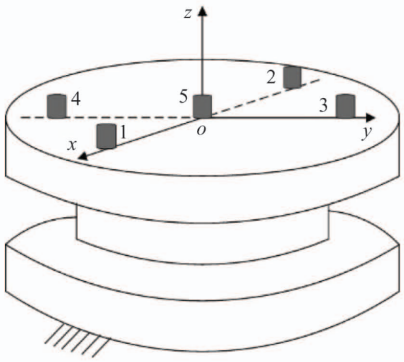

Fig. 11 The schematic diagram of force-loading disposal

4 Online-static calibration method

The following experiment uses online-static calibration method, which is shown in Fig. 10. The online-static calibration method can reduce the gravity error caused by the change of sensor attitude. Fig. 11 shows the distribution of sensor calibration loading points, where the distances between 1, 2, 3, 4 and the origin are all l, and they are symmetric about the origin of the base coordinate system.

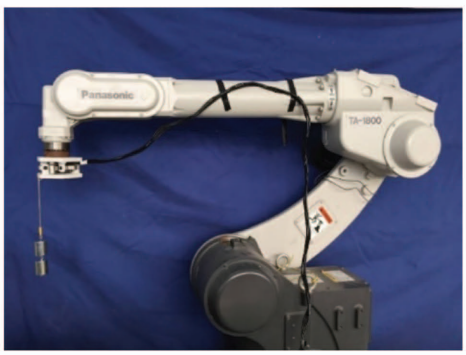

Fig. 10 System of prototype online-static calibration testing

Loading and unloading 20 times in each direction to be calibrated, the force/torque loading value is 2 N/50 N · mm (Force/Torque). When loading the external force in the positive direction of the x-axis, the hooked weight is suspended at the loading point 2, and the load gravity is G_2. Then, by adjusting the position of the robot, the suspension of the sensor hooked weight can pass vertically through the loading point 1 only under the hooked weight, which is shown in Fig. 12(a). At this time, the positive direction of the x-axis is vertically downward in the direction of gravity, and the sensor is only subjected to the load force F_x along the positive direction of the x-axis, where $F_x = G_2$. The external force loading method in the negative direction of the x-axis is similar to the loading in the positive direction.

Fig. 12(b) shows x-axis positive direction torque loading diagram. By adjusting the posture of the robot, the sensor force platform is vertically downward, and the hooked weight is hung at the loading point 3. The load gravity is G_3. At this time, the sensor is not only

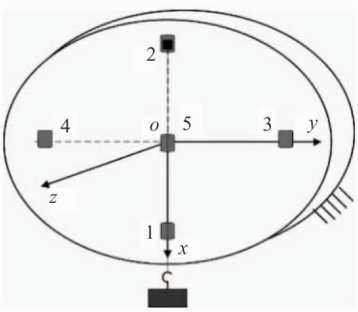

(a) x-axis force loading

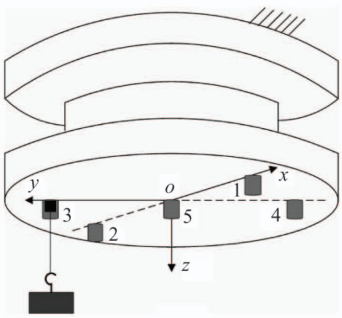

(b) x-axis force moment loading

Fig. 12 The schematic diagram of x-axis positive direction force/torque loading

subjected to the load moment M_x in the positive direction of the x-axis, but also receives the load force F_z in the positive direction of the z-axis, where $M_x = lG_3$, $F_z = G_3$. The external torque loading method in the negative direction of the x-axis is similar to the loading in the positive direction, and the external force/torque online loading method of the y-axis is similar to the x-axis.

When loading the force in the positive direction of the z-axis, the force-measuring platform is vertically

downward by adjusting the position of the robot, and the positive direction of the z-axis is vertically downward along the direction of gravity, which is shown as Fig. 13(a). The hooked weight is hung at load point 5 and the load gravity is G_5. At this point the sensor is only subjected to the z-axis forward load force F_z and F_z is equal to G_5. The external force loading method in the negative direction of the z-axis is similar to the loading in the positive direction.

Fig. 13(b) shows the schematic diagram of z-axis positive direction torque loading. Firstly, the hooked weight is hung at the loading point 2, and the position of the robot is adjusted so that the hanging line of the hook point of the loading point 2 can pass vertically through the loading point 1 only under the gravity of the hooked weight.

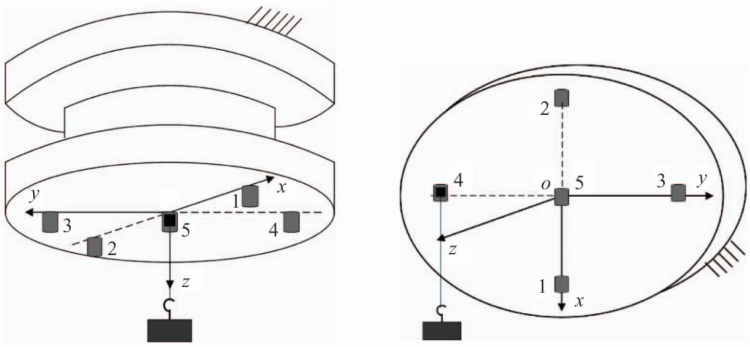

(a) z-axis force loading (b) z-axis force moment loading

Fig. 13 The schematic diagram of z-axis positive direction force/torque loading

At this time, the positive direction of the x-axis of the sensor is along the direction of gravity. Then, after adjusting the sensor attitude, remove the hooked weight of the loading point 2, and hang the hooked weight at the loading point 4. The load gravity is G_4. At this point the sensor is subjected to a positive load moment M_z around the z-axis, with $M_z = lG_4$, and is also subjected to a load F_x along the positive direction of the x-axis, with $F_x = G_4$. The external torque loading method in the negative direction of the z-axis is similar to the loading in the positive direction.

5 Static calibration experiment results

A series of calibration experiments for sensor prototypes yielded 240 sets of data by loading/unloading 20 times at each load point. According to the measurement results, the static calibration matrix of orthogonal-parallel six-axis force/torque sensor in Eq. (11) can be obtained as

$$\boldsymbol{G}_c = \begin{bmatrix} -0.038 & 0.083 & 0.001 & -0.120 & 0.549 & -0.460 \\ 0.048 & 0.022 & -0.020 & -0.497 & 0.135 & 0.287 \\ 0.175 & 0.176 & 0.177 & 0.100 & 0.091 & -0.007 \\ -11.771 & 14.844 & -1.057 & -18.029 & 12.274 & 5.650 \\ -9.053 & -5.296 & 10.134 & -0.486 & -6.792 & 5.621 \\ 1.020 & -2.358 & -0.555 & -7.830 & -14.268 & -13.130 \end{bmatrix} \tag{16}$$

The linearity matrix of the prototype is obtained by analyzing the data according to Eq. (12) – Eq. (15), which can be obtained as

$$\boldsymbol{E}_L = \begin{bmatrix} 0.0651 & 0.0478 & 0.0247 & 0.0799 & 0.0286 & 0.0551 \\ 0.0093 & 0.0413 & 0.0378 & 0.0267 & 0.0197 & 0.0362 \\ 0.0100 & 0.0158 & 0.0225 & 0.0274 & 0.0299 & 0.0102 \\ 0.0147 & 0.0590 & 0.0143 & 0.0098 & 0.0333 & 0.0093 \\ 0.0049 & 0.0290 & 0.0118 & 0.0175 & 0.0303 & 0.0257 \\ 0.0237 & 0.0088 & 0.0104 & 0.0205 & 0.0057 & 0.0141 \end{bmatrix} \tag{17}$$

The maximum type I measurement error of the prototype is 6.51% and the maximum type II measurement error is 7.99% within the full scales of force and torque measurements, which can be obtained according to Eq. (17).

It can be seen that the prototype has good linearity in the six main directions of measurement and the coupling direction. The experimental results show that the prototype can obtain better measurement accuracy in the actual measurement. Compared with the existing commercial sensor, the developed six-axis force/torque sensor prototype can meet the requirements of industrial production in precision measurement.

6 Conclusion

The optimal design and experiment research of an orthogonal-parallel six-axis force/torque sensor have been conducted. Through measuring limbs horizontal and vertical arrangement, the orthogonal-parallel six-axis force/torque sensor can achieve decoupling measurement. It is optimized based on the actual working

condition function of the sensor. The sensor prototype is manufactured as the optimized structural parameters and the calibration system is developed. An online-static calibration method is proposed which can reduce the gravity error caused by the sensor attitude change. The experimental result shows that the maximum nonlinearity error in all the directions and the maximum interference error are less than 8.00% within the full scales of force and torque measurements, which indicates that the developed six-axis force/torque sensor by optimal design possesses good performance. The study is helpful for the further research and practical application of the orthogonal-parallel six-axis force/torque sensor.

References

[1] Zhou S, Sun J, Gao F. Influence of flexible spherical joints parameters on accuracy of the six-axis force/torque sensor with three-three orthogonal parallel mechanism[J]. *Mechanism and Machine Theory*, 2020, 145:103697

[2] Li H J, Song A G, Li A, et al. Static calibration and decoupling for six-axis force/torque sensors based on genetic algorithm[J]. *Journal of Nanoelectronics and Optoelectronics*, 2019, 14: 431-441

[3] Song W, Li C, Wang C, et al. Force/moment isotropy of 8/4-4 parallel six-axis force sensor based on performance atlases[J]. *Transactions of Nanjing University of Aeronautics and Astronautics*, 2018, 35(6):1018-1026

[4] Merlet J P. Parallel Robots[M]. Second Edition. Berlin: Springer, 2006: 265-266

[5] Fujii Y. Toward dynamic force calibration[J]. *Measurement*, 2009, 42: 1039-1044

[6] Li Y J, Wang G C, Zhao D, et al. Research on a novel parallel spoke piezoelectric 6-DOF heavy force/ torque sensor[J]. *Mechanical Systems and Signal Processing*, 2013, 36(1): 152-167

[7] Li Y J, Yang C, Wang G C, et al. Research on the parallel load sharing principle of a novel self-decoupled piezoelectric six-dimensional force sensor[J]. *ISA Transactions*, 2017, 70: 447-457

[8] Hirosea K, Dokia H, Kondoa A. Dynamic analysis and motion measurement of ski turns using inertial and force sensors[J]. *Procedia Engineering*, 2013, 60: 355-360

[9] Yuan C, Luo L P, Yuan Q, et al. Development and evaluation of a compact 6-axis force/moment sensor with a serial structure for the humanoid robot foot[J]. *Measurement*, 2015, 70: 110-122

[10] Li Y J, Wang G C, Yang X, et al. Research on static decoupling algorithm for piezoelectric six axis force/torque sensor based on LSSVR fusion algorithm[J]. *Mechanical Systems and Signal Processing*, 2018, 110: 509-520

[11] Gao W, Jia C, Jiang Z, et al. The design and analysis of a novel micro force sensor based on depletion type movable gate field effect transistor[J]. *Journal of Microelectromechanical Systems*, 2019, 99:1-13

[12] Wang Z J, He J, Cui B Y, et al. Dynamic analysis of double-layer and pre-stressed multi-limb six-axis force sensor[J]. *High Technology Letters*, 2019, 25(2):189-196

[13] Kebede G A, Ahmad A R, Lee S C, et al. Decoupled six-axis force-moment sensor with a novel strain gauge arrangement and error reduction techniques[J]. *Sensors*, 2019, 19(13):3012

[14] Wang Z J, Li Z X, He J, et al. Optimal design and experiment research of a fully pre-stressed six-axis force/torque sensor[J]. *Measurement*, 2013, 46(6): 2013-2021

Wang Zhijun, born in 1983. He received his B.S. and Ph.D degrees in mechanical-electronic engineering from Yanshan University in 2006 and 2012 respectively. His research interests include the robotic mechanism, six-axis force sensor and robot control technology.